DOI: 10.1038/NGEO444

Supplementary Figure captions:

Figure S1: a) Time-latitude diagram of precipitation (mm day^{-1}) from CMAP (1979-2005), averaged between 35°-45°W. b) as in a) but for ECHAM-4 control run.

Figure S2: Seasonal cycle of a) precipitation and b) $\delta^{18}O$ in NE Brazil for control run and mid-Holocene (6 ky B.P). as simulated with ECHAM-4. The seasonal cycle of precipitation from CMAP is shown for comparison. Data for ECHAM-4 and CMAP was extracted over grid cell closest to cave sites.

Figure S3: Schematic diagrams showing the summer (DJF) precipitation patterns in South America and related changes in Walker and Hadley circulation for the periods corresponding to a) High summer insolation in southern hemisphere during the last 4,000 years (late Holocene) and b) Low summer insolation in southern hemisphere between 9,000 and 6,000 years (early and mid-Holocene).

Figure S4: a) Difference in austral summer and fall (DJFMAM) vertical velocity and horizontal divergence between 6 ky B.P. and present as simulated with ECHAM-4, averaged between 0° and 10°S along an west-east transect from 90°W to 50°E. Vertical velocity is indicated by shading (see scale below) and white contours (contour interval is $1.5 \cdot 10^{-2}$ Pa s^{-1}). Horizontal divergence is shown by black (positive) and gray (negative) contours; contour interval is $5 \cdot 10^{-7}$ s^{-1}; 0-contour is omitted). b) as in a) except vertical and zonal wind components are plotted instead of divergence. Scale for wind components are shown in lower left. Black bars at bottom of Figures indicate location of South America and Africa respectively.

Figure S5: Plot of age versus depth for stalagmites collected in Rainha, Furna Nova and Abissal caves, a) FN1 Stalagmite, b) RN1 Stalagmite, c) RN4 Stalagmite, d)Abissal Stalagmite. Error bars indicate 2σ error.

DOI: 10.1038/NGEO444

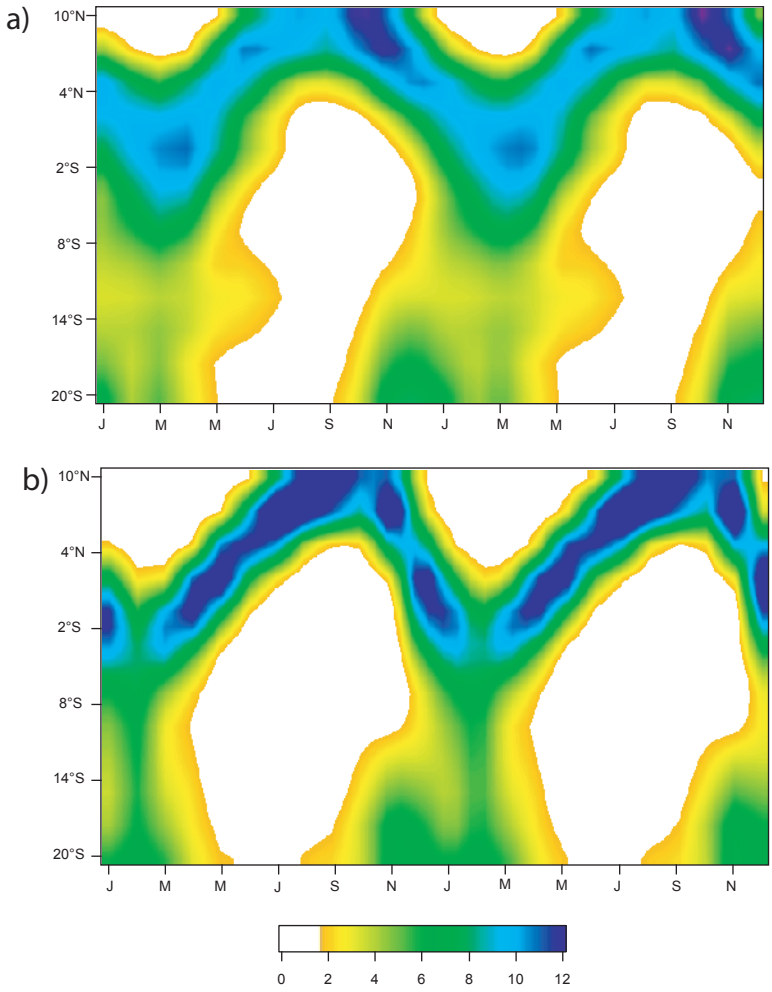

Figure S1: a) Time-latitude diagram of precipitation (mm day^{-1}) from CMAP (1979-2005), averaged between 35°-45°W. b) as in a) but for ECHAM-4 control run.

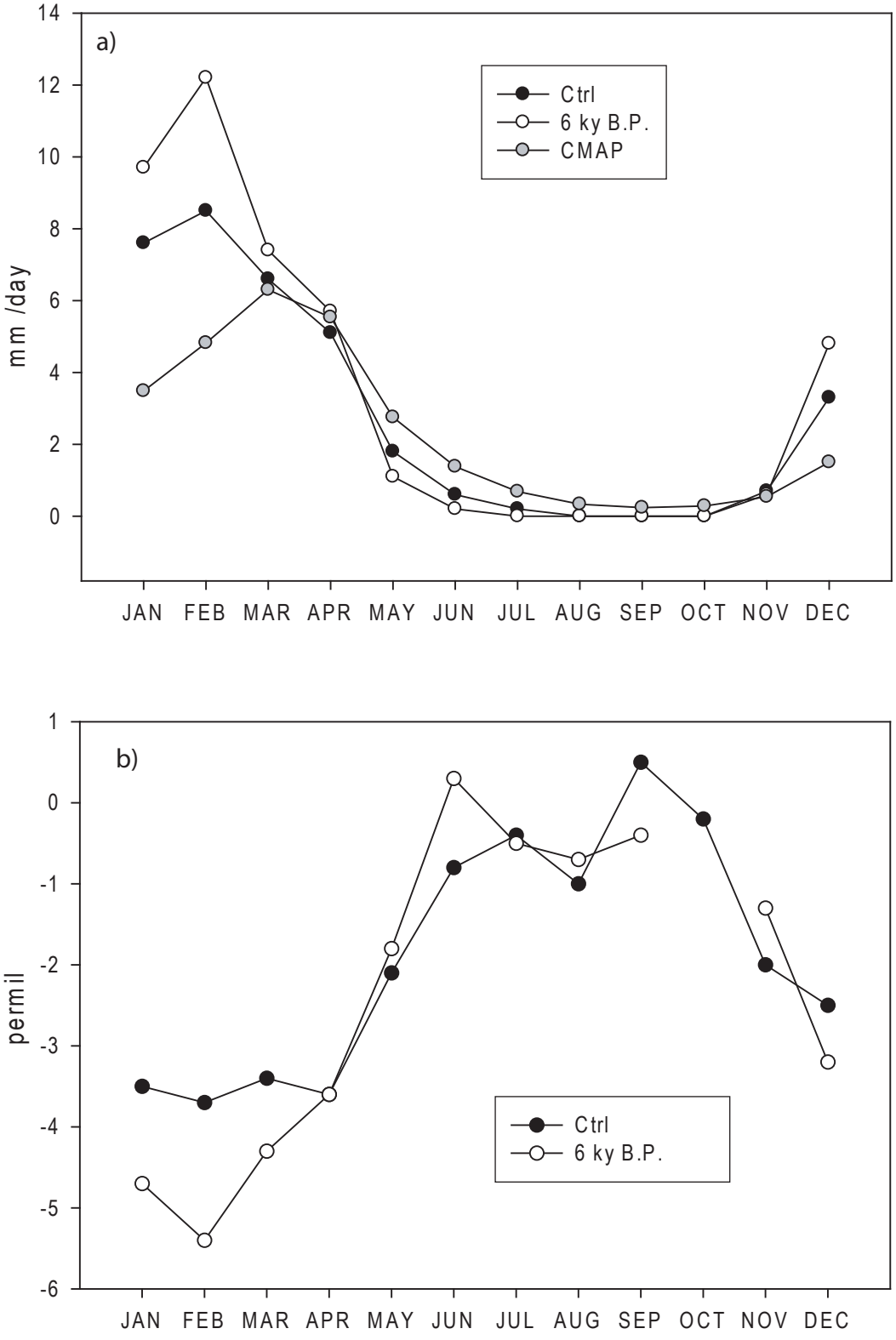

Figure S2: Seasonal cycle of a) precipitation and b) $\delta^{18}O$ in NE Brazil for control run and mid-Holocene (6 ky B.P). as simulated with ECHAM-4. The seasonal cycle of precipitation from CMAP is shown for comparison. Data for ECHAM-4 and CMAP were extracted over grid cell closest to cave sites.

DOI: 10.1038/NGEO444

SUPPLEMENTARY INFORMATION

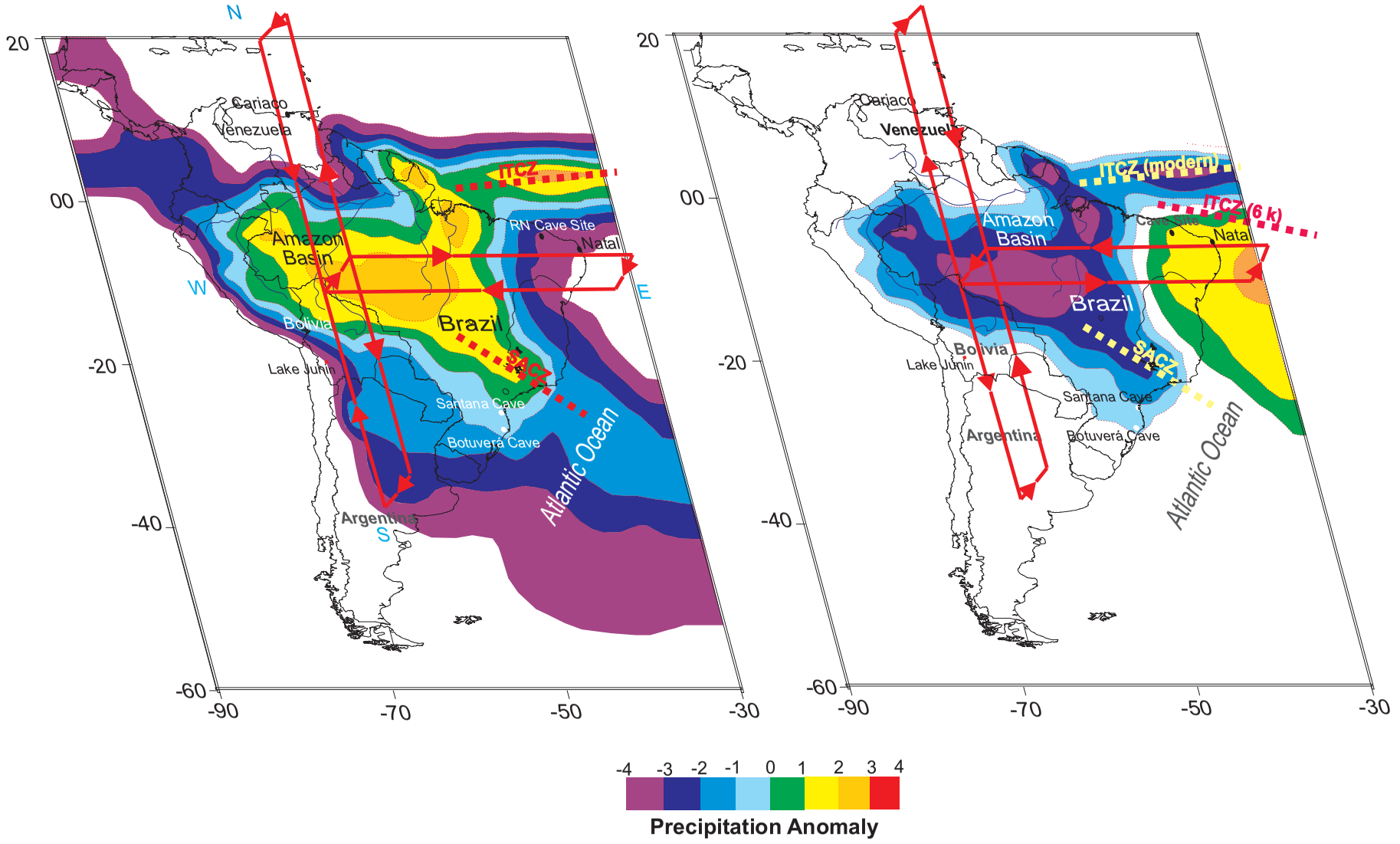

Figure S3: Schematic diagrams showing the precipitation patterns of the summer in South America (DJF) and related changes in Walker and Hadley circulation for the periods correspondent to a) High summer insolation in southern hemisphere during the last 4,000 years (late Holocene) and b) Low summer insolation in southern hemisphere between 9,000 and 6,000 years (early and mid-Holocene).

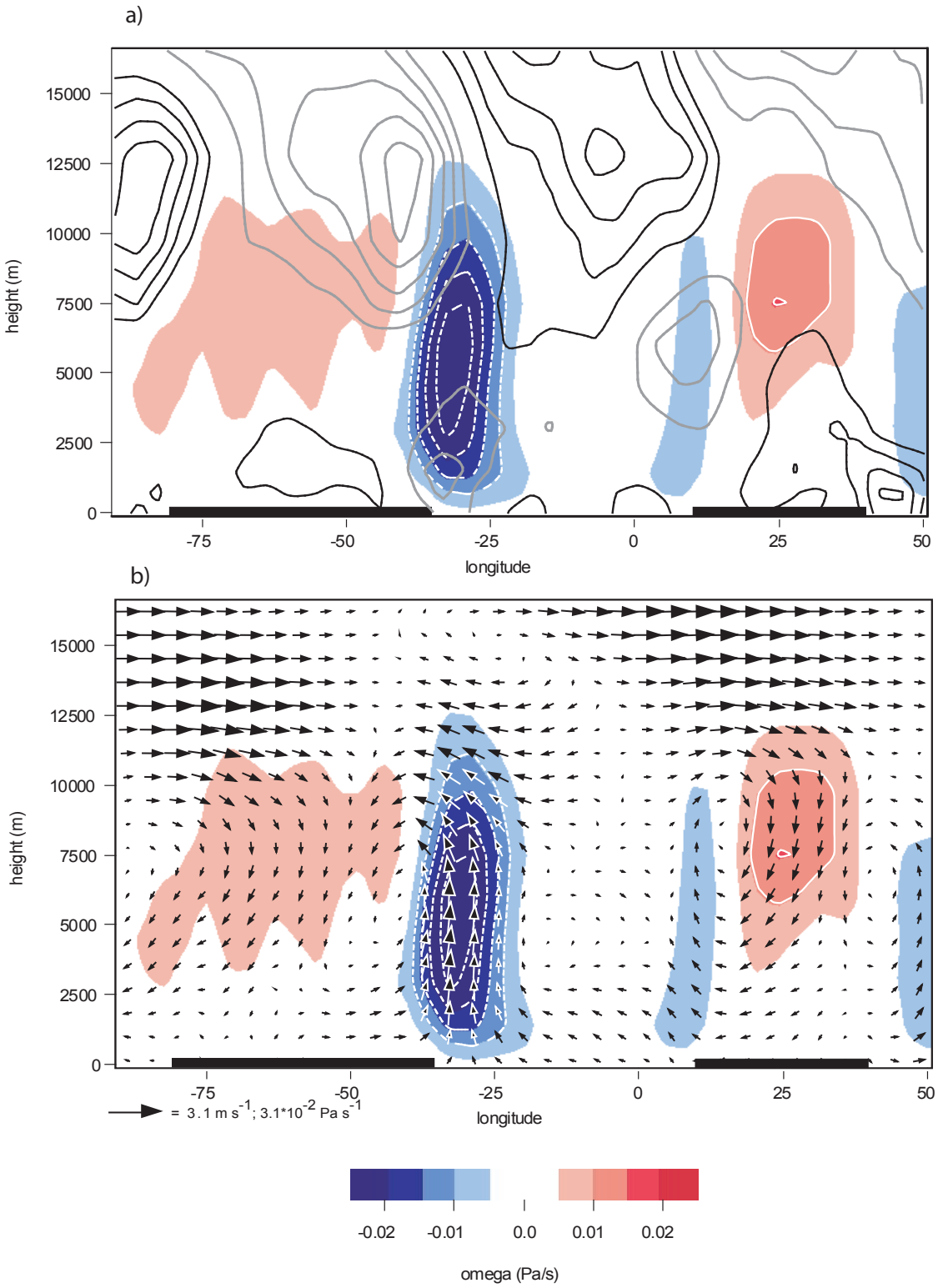

Figure S4: a) Difference in austral summer and fall (DJFMAM) vertical velocity and horizontal divergence between 6 ky B.P. and present as simulated with ECHAM-4, averaged between 0° and 10°S along an west-east transect from 90°W to 50°E. Vertical velocity is indicated by shading (see scale below) and white contours (contour interval is $1.5 \cdot 10^{-2}$ Pa s^{-1}). Horizontal divergence is shown by black (positive) and gray (negative) contours; contour interval is $5 \cdot 10^{-7}$ s^{-1}; 0-contour is omitted). b) as in a) except vertical and zonal wind components are plotted instead of divergence. Scale for wind components are shown in lower left. Black bars at bottom of Figures indicate location of South America and Africa respectively.

DOI: 10.1038/NGEO444

SUPPLEMENTARY INFORMATION

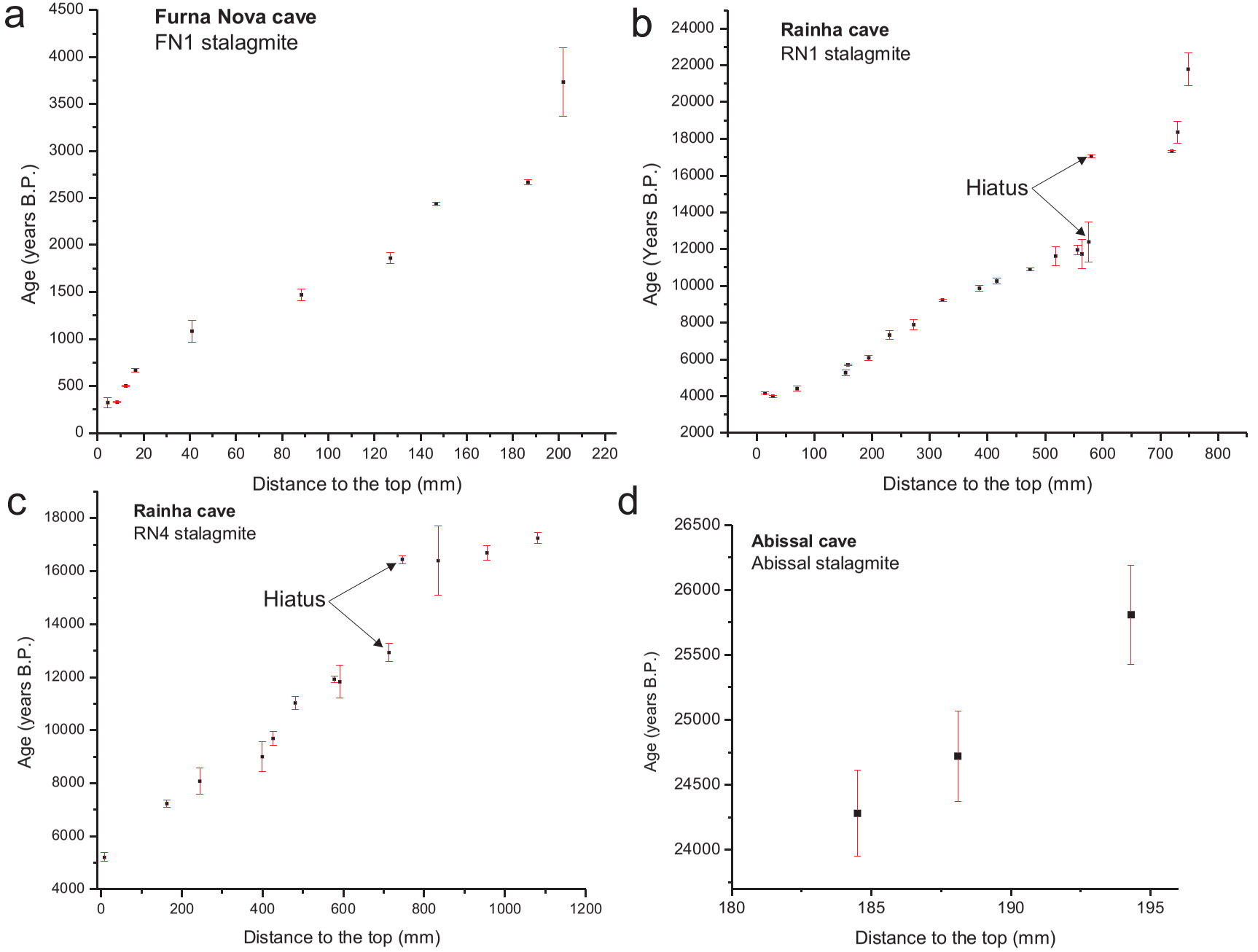

Supplemental Figure 5. Plot of age versus depth for stalagmites collected in Rainha, Furna Nova and Abissal caves a) FN1 Stalagmite, b) RN1 Stalagmite, c) RN4 Stalagmite, d)Abissal Stalagmite. Error bars indicate 2σ error.

DOI: 10.1038/NGEO444

Supplemental Table 1

Sample Number	Depth (mm)	^{238}U (ppb)	^{232}Th (ppt)	$^{230}Th / ^{232}Th$ (atomic x10^{-6})	$\delta^{234}U$* (measured)	$^{230}Th / ^{238}U$ (activity)	^{230}Th Age (yr) (uncorrected)	^{230}Th Age (yr) (corrected)	$\delta^{234}U_{Initial}$** (corrected)
FN1 - Stalagmite									
FN1-a	5	119.3 ± 0.2	228 ± 2	28 ± 4	-68 ± 3	0.0033 ± 0.0004	383 ± 50	323 ± 58	-68 ± 3
FN1-b	9	4134 ± 16	698 ± 2	280 ± 5	-58 ± 1	0.00288 ± 0.00005	333 ± 6	328 ± 6	-58 ± 1
FN1-B1	12	7837 ± 26	3878 ± 10	148 ± 2	-58 ± 2	0.00443 ± 0.00006	515 ± 7	500 ± 10	-58 ± 2
FN1-T	16	1152 ± 4	1256 ± 3	91 ± 1	-61 ± 2	0.00601 ± 0.00007	700 ± 9	666 ± 19	-61 ± 2
FN1-2	41	48.1 ± 0.1	151 ± 2	54 ± 5	-53 ± 2	0.0102 ± 0.0009	1180 ±100	1080 ±110	-53 ± 2
FN1-3	88	85.5 ± 0.1	209 ± 1	90 ± 3	-56 ± 2	0.0133 ± 0.0004	1545 ±48	1469 ±61	-56 ± 2
FN1-4	127	75.3 ± 0.2	97 ± 1	210 ± 7	-53 ± 3	0.0164 ± 0.0005	1899 ±54	1860 ±57	-53 ± 3
FN1-4A	147	17533 ± 81	3486 ± 7	1734 ± 6	-55 ± 2	0.0209 ± 0.0001	2441 ±14	2435 ±14	-56 ± 2
FN1-B	187	20240 ± 200	2847 ± 8	2680 ± 12	-55 ± 3	0.0229 ± 0.0002	2671 ±30	2667 ±30	-55 ± 3
FN1-4B	202	7297 ± 22	165820 ± 830	27 ± 1	-52 ± 2	0.0377 ± 0.0008	4435 ±91	3730 ±360	-52 ± 2
RN1-stalagmite									
RN1-1a	14	115.4 ±0.2	222 ±12	366 ±20	110 ±1	0.0427 ±0.0003	4275 ±30	4167 ±47	112 ±1
RN1-1b	28	119.4 ±0.2	272 ±11	299 ±13	113 ±2	0.0413 ±0.0003	4117 ±32	4001 ±53	114 ±2
RN1-2a	70	64.9 ±0.2	480 ±11	104 ±3	108 ±2	0.0466 ±0.0004	4674 ±45	4420 ±140	109 ±2
RN1-4c	154	65.8 ±0.1	489 ±15	121 ±4	101 ±2	0.0545 ±0.0005	5528 ±51	5280 ±150	103 ±2
RN1-4d	158	96.3 ±0.2	233 ±10	389 ±16	99 ±2	0.0573 ±0.0003	5828 ±34	5707 ±56	101 ±2
RN1-6a	194	115.9 ±0.2	943 ±11	126 ±2	99 ±2	0.0624 ±0.0003	6364 ±28	6090 ±150	101 ±2
RN1-7a	230	221.4 ±0.4	2868 ±29	96 ±1	100 ±1	0.0754 ±0.0002	7728 ±26	7330 ±240	102 ±1
RN1-8a	272	193.1 ±0.3	3000 ±31	86 ±1	96 ±1	0.0811 ±0.0002	8360 ±28	7890 ±290	98 ±1
RN1-10a	322	113.9 ±0.2	187 ±5	898 ±24	90 ±2	0.0895 ±0.0003	9328 ±38	9228 ±49	92 ±2
RN1-12a	386	284.3 ±0.6	2447 ±25	187 ±2	95 ±2	0.0976 ±0.0003	10154 ±36	9870 ±170	98 ±2
RN1-13a	416	188.6 ±0.4	1632 ±17	193 ±2	95 ±2	0.1012 ±0.0003	10552 ±42	10270 ±170	97 ±2
RN1-15b	474	74.0 ±0.1	216 ±5	605 ±15	109 ±2	0.1070 ±0.0004	11041 ±47	10909 ±72	112 ±2
RN1-17d	518	25.6 ±0.1	694 ±9	73 ±1	113 ±2	0.1198 ±0.0007	12379 ±85	11620 ±510	117 ±2
RN1-19c	556	16.90 ±0.02	227 ±5	148 ±3	123 ±2	0.1206 ±0.0008	12360 ±88	11960 ±260	127 ±2
RN1-20b	564	17.24 ±0.03	721 ±12	49 ±1	118 ±2	0.1249 ±0.0014	12876 ±154	11730 ±790	122 ±2
RN1-21a	576	31.0 ±0.1	1826 ±27	38 ±1	122 ±3	0.1358 ±0.0015	14028 ±174	12400 ±1100	126 ±3
RN1-22c	580	35.3 ±0.1	64 ±5	1490 ±110	133 ±2	0.1657 ±0.0007	17166 ±79	17063 ±85	140 ±2
RN1-27b	720	167.7 ±0.3	326 ±5	1424 ±24	135 ±1	0.1683 ±0.0004	17435 ±51	17329 ±62	141 ±1

DOI: 10.1038/NGEO444

RN1-28b	730	482.7 ±0.7	16470 ±170	90 ±1	140 ±1	0.1856 ±0.0004	19284 ±54	18360 ±620	148 ±1
RN1-29e	748	212.9 ±0.2	10570 ±110	72 ±1	134 ±1	0.2178 ±0.0005	23132 ±65	21800 ±900	143 ±1
Ale 1 -stalagmite									
Ale1-1	0	35.7 ± 0.2	266 ± 2	335 ± 7	151 ± 10	0.152 ± 0.003	15360 ±350	15170 ±360	157 ± 10
Ale1-4	510	117.3 ± 0.4	249 ± 2	1322 ± 12	154 ± 4	0.171 ± 0.001	17370 ±160	17310 ±160	161 ± 4
Abissal stalagmite									
ABIS-10B	185	60.6 ± 0.2	322 ± 2	738 ± 8	177 ± 6	0.238 ± 0.002	24410 ±320	24280 ±330	190 ± 7
ABIS-10C	188	52.9 ± 0.1	526 ± 2	402 ± 5	177 ± 4	0.242 ± 0.003	24960 ±330	24720 ±350	190 ± 4
ABIS-B	194	201.1 ± 0.5	3977 ± 14	211 ± 2	175 ± 4	0.253 ± 0.002	26290 ±290	25810 ±380	188 ± 4
RN4-stalagmite									
RN4-1	8	146.5 ± 0.4	1719 ± 4	76 ± 1	100 ± 2	0.0544 ± 0.0004	5522 ±47	5210 ±160	101 ± 3
RN4-2	162	69.4 ± 0.1	668 ± 2	125 ± 1	94 ± 2	0.0727 ± 0.0006	7490 ±70	7230 ±150	96 ± 2
RN4-2a	244	80.0 ± 0.2	2122 ± 26	53 ± 1	89 ± 2	0.0850 ± 0.0005	8845 ±57	8080 ±500	91 ± 2
RN4-3	399	117.9 ± 0.3	4824 ± 16	39 ± 1	92 ± 3	0.0967 ± 0.0012	10100 ±140	9000 ±570	94 ± 3
RN4-3a	425	144.6 ± 0.3	1909 ± 25	121 ± 2	93 ± 2	0.0969 ± 0.0004	10097 ±46	9690 ±250	96 ± 2
RN4-4	481	54.1 ± 0.1	835 ± 2	118 ± 1	109 ± 4	0.1106 ± 0.0014	11430 ±160	11030 ±260	113 ± 4
RN4-4a	577	36.7 ±0.1	191 ±10	370 ± 19	113 ± 1	0.1168 ± 0.0007	12056 ±81	11920 ±130	117 ± 2
RN4-5	591	38.4 ± 0.1	1717 ± 4	46 ± 1	113 ± 3	0.1255 ± 0.0016	13000 ±190	11830 ±620	117 ± 3
RN4-6	713	95.5 ± 1.2	1346 ± 3	151 ± 1	125 ± 17	0.1294 ± 0.0019	13290 ±300	12930 ±340	129 ± 17
RN4-7	746	56.3 ±0.1	454 ±5	328 ±4	126 ± 1	0.1605 ± 0.0004	16706 ±47	16440 ±150	132 ± 1
RN4-8	835	53.3 ±0.1	3925 ±40	39.4 ±0.4	130 ± 1	0.1762 ± 0.0005	18400 ±63	16400 ±1300	137 ± 2
RN4-9	956	75.2 ±0.1	1120 ±12	183 ±2	133 ± 1	0.1653 ± 0.0004	17125 ±54	16690 ±270	140 ± 1
RN4-10	1082	87.1 ± 0.2	1005 ± 3	238 ± 2	119 ± 3	0.1669 ± 0.0013	17540 ±150	17240 ±210	125 ± 3

Analytical errors are 2σ of the mean.

[a] $\delta^{234}U = ([^{234}U/^{238}U]_{activity} - 1) \times 1000$.

[b] $\delta^{234}U_{initial}$ corrected was calculated based on ^{230}Th age (T), i.e., $\delta^{234}U_{initial} = \delta^{234}U_{measured} X\ e^{\lambda 234*T}$, and T is corrected age.

[c] $[^{230}Th/^{238}U]_{activity} = 1 - e^{-\lambda_{230}T} + (\delta^{234}U_{measured}/1000)[\lambda_{230}/(\lambda_{230} - \lambda_{234})](1 - e^{-(\lambda_{230} - \lambda_{234})T})$, where T is the age.

Decay constants are 9.1577×10^{-6} yr^{-1} for ^{230}Th, 2.8263×10^{-6} yr^{-1} for ^{234}U, and 1.55125×10^{-10} yr^{-1} for ^{238}U (Cheng et al., 2000).

[d] The degree of detrital ^{230}Th contamination is indicated by the $[^{230}Th/^{232}Th]$ atomic ratio instead of the activity ratio.

[e] Age corrections were calculated using an average crustal $^{230}Th/^{232}Th$ atomic ratio of $4.4 \times 10^{6} \pm 2.2 \times 10^{-6}$.

Those are the values for a material at secular equilibrium, with the crustal $^{232}Th/^{238}U$ value of 3.8. The errors are arbitrarily assumed to be 50%.